MEBT-BI-FC91-02

Thermo-Mechanical Analysis of the ESS MEBT FC

A. R. Páramo, F. Sordo, I. Bustinduy

04 July 2017

Project: MEBT
Version: 0.2
Approved by: I. Bustinduy
Revised by: F. Sordo

Change History

Rev.	Date	Author(s)	Description
0.1	2017-06-19	A. R. Páramo	First Version
0.2	2017-07-04	A. R. Páramo	Minor Changes

Thermo-Mechanical Analysis of the ESS MEBT FC

A. R. Páramo[1*], F. Sordo[2], I. Bustinduy[1]

[1] Accelerator/Control & Diagnostics Group, ESS-Bilbao, Spain

[2] Target Group, ESS-Bilbao, Spain

[*]Corresponding author: arparamo@essbilbao.org

Abstract.

In this report, we study the thermomechanical response of the MEBT FC during operation.

We study its behaviour for the operational conditions expected during MEBT commissioning phase. First, we address how the beam irradiation on the graphite collector can be withstood, operating below graphite strength limit.

Then we address operation in the steady state. We specifically address thermal contact conditions, comparing the use of stainless steel (SS) or copper (Cu) as the substrate material. The analysis shows that thermal contact between the different components is the defining factor. We estimate the thermal contact as function of the contact force, and specify contact requirements for the FC. Finally, we estimate the refrigeration parameters required for MEBT FC.

1. Introduction

This work studies the temperature, deformation and stresses that appear during operation in the FC of the MEBT. In Figure 1 the layout of the MEBT beam instrumentation is shown.

The Faraday Cup is designed in order to measure the beam current in the ESS MEBT [1].

In the ESS MEBT Preliminary Design Review (PDR) [1, 2] it was shown that graphite is the chosen material to withstand irradiation. However, the substrate material was not yet decided, for its selection contact conditions and mechanical constraints have to be taken into account.

We specifically study the use of copper or steel as the substrate material. On one side copper offers excellent thermal properties but a more difficult fabrication process, while the use of steel results in only acceptable thermal properties but a simple fabrication process. We do the study for the nominal operation conditions for the in the MEBT.

In the MEBT the beam has a nominal intensity of 62.5 mA with 3.63 MeV of energy. The FC is designed to fulfil ESS commissioning modes [3]:

- Mode I: Fast tuning is used for steady state analysis, the average power if 16 W, for pulses of 5 μs at 14 Hz.
- Mode II: Slow Tuning is used in the transient analysis. The coating materials have to withstand ~230 kW during 50 μs with at frequency of 1 Hz, for an average power of 11 W.

As shown in Table 4, for Mode II the pulse duration is larger and we use this mode for analysis of the transient thermo-mechanical effects of irradiation in Section 3. In Mode I the average beam power is higher and we use this mode for defining the steady state operation conditions in Section 4.

The materials used in this work are a) Graphite R4550 for facing irradiation, b) Pure Copper or SS316 as substrate material and c) High purity alumina as insulator in the FC. The properties of the materials are described in Appendix A: Material Properties.

.

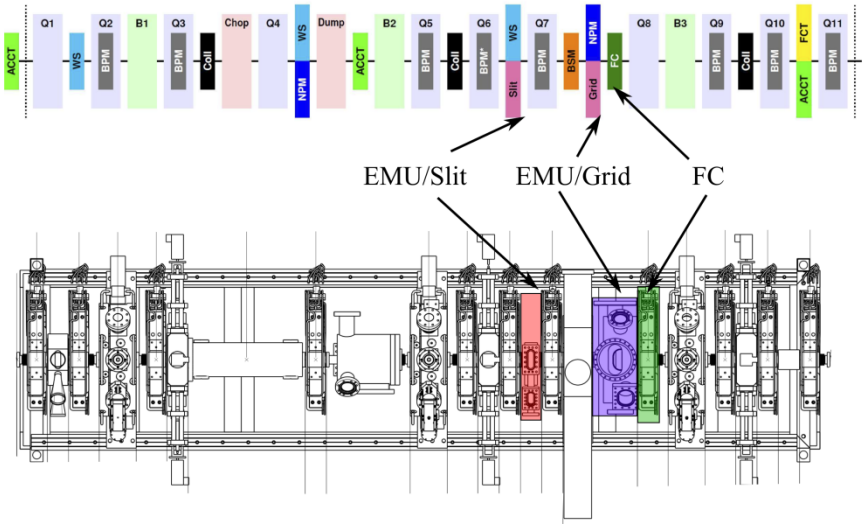

Figure 1: Top) Block diagram of the ESS-MEBT. Bottom) Layout of the ESS-MEBT.

Table 1: Beam Parameters in the FC.

Parameter	Value		Parameter		Value	
Proton Energy	3.63	MeV	Beam Size	σ_x	2.488	mm
Intensity	62.5	mA		σ_y	2.624	mm
Mode I: Fast Tuning	5 µs - 14 Hz -16 W					
Mode II: Slow Tuning	50 µs - 1 Hz - 11 W					

2. **Design Criteria**

We can divide the analysis in two stages, the *i)* transient analysis which studies the beam irradiation effects on the collector during the pulse duration, and *ii)* the steady state analysis that studies the heating of the product over operation with times of minutes.

As a first approximation, the thermo-mechanical effects can be estimated as:

$$\Delta T = \Delta T_{steady} + \Delta T_{transient} \quad (1)$$

$$\Delta \sigma = \Delta \sigma_{steady} + \Delta \sigma_{\text{transient}}$$

As we will show in the next sections (Sections 3 and 4), for the graphite collector the most intense effects take place during the transient, and the steady state can be almost neglected. For the rest of components only the study of the steady state is relevant.

In order to operate with a safe limit avoiding failure, we apply a design criteria [2, 4].

- $\sigma_{Max} \leq \frac{2}{3}\sigma_{strength}$

We use Tresca criterion for graphite with a maximum stress intensity of $2/3 \cdot 125 = 83$ MPa [4, 5], and the Von Mises criteria for metals. For the material limits see Appendix A: Material Properties.

Regarding the temperature in the case of metals a general rule $T_{Max} \leq \frac{1}{3}T_{Melt}$ can be used. This general rule guarantees low operational temperatures, which is important in order to avoid temperature effects (recrystallization) that lower the structural strength of the material. In the case of graphite, the strength increases at high temperatures [5], and the temperature criterion can be relaxed.

3. Transient Analysis

3.1. Model Description

In Figure 2 we show the Ansys FEM model used in this analysis. We simulate a plate of 8 mm of thickness, with sides of 25 mm. The material used in this work is Graphite R4550, see Appendix A: Material Properties.

The mesh is refined in the irradiated surface in order to reproduce the Bragg Peak. Regarding mechanical boundary conditions, symmetry conditions and a fixed support in the back of the plate are applied.

Regarding thermal conditions, the analysis studies irradiation on a plate with a uniform temperature of 22 C. No cooling conditions or radiative effects are included, which results in a conservative estimation.

The thermal load is introduced from simulations in MCNPX with the proton beam characterized by a Gaussian profile:

$$I''(x,y) = \frac{I_o}{2\pi\sigma_x\sigma_y} \cdot e^{-\frac{x^2}{2\sigma_x^2}} \cdot e^{-\frac{x^2}{2\sigma_y^2}} \quad (2)$$

In order to characterize beam deposition, we define the integrated current (I_c) as the total current flux over pulse irradiation:

$$I_c = \frac{I_o}{2\pi\sigma_x\sigma_y/\sin(\alpha)} \cdot \tau \quad (3)$$

Where I_0 is the beam current, σ_x, σ_y the beam size, α the incident angle and τ de pulse duration.

In Table 2 we show the irradiation conditions expected in the FC for a perpendicular beam of size σ_x=σ_y=0.25 cm. In order to estimate the power density (W/m^3) we multiply the current flux (A/m^2) by the stopping power (eV/m). Finally, the energy deposition (J/m^3) is calculated multiplying the power density by the pulse duration.

In Figure 3 the stopping power in graphite for different incident angles is shown. We observe that the Bragg Peak for perpendicular graphite appears at ~130 μm. We observe that the that the stopping power and penetration depth scales inversely to the angle.

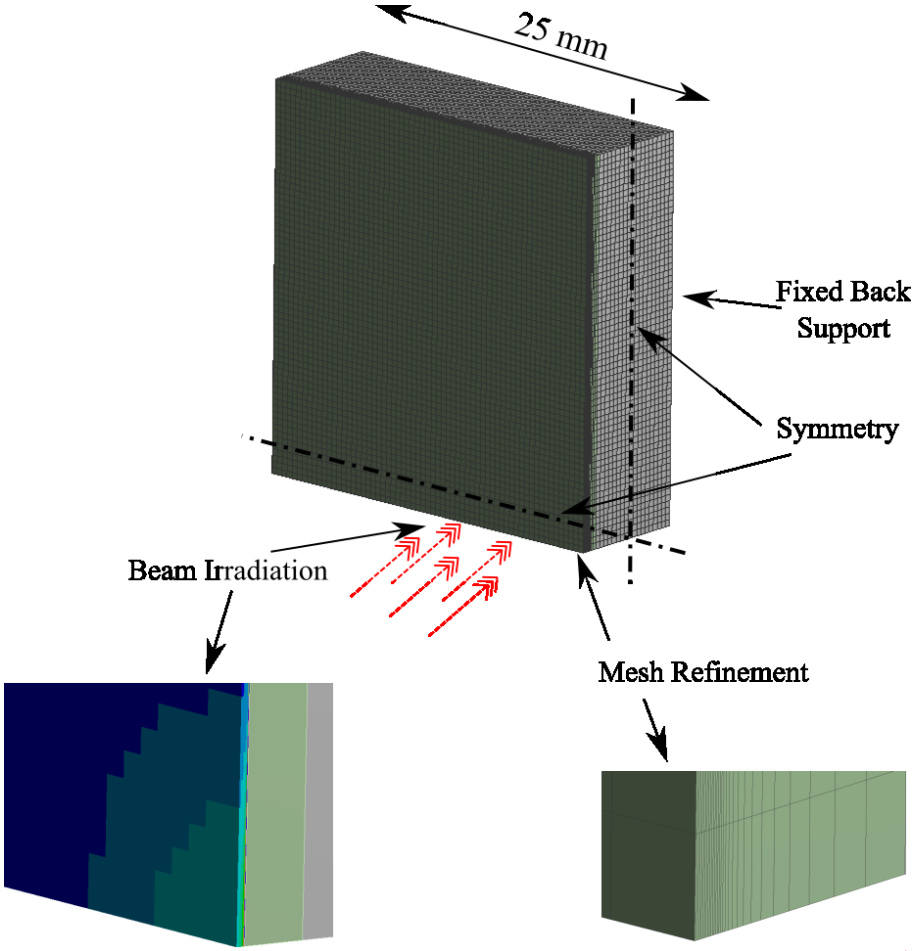

Figure 2: FEM model used in this work.

Table 2: Irradiation Conditions in perpendicularly irradiated graphite for the FC in the commissioning mode.

Parameter	Value
Proton Energy (MeV)	3.63
Beam Current (mA)	62.5
Pulse duration (μs)	50
Pulse Energy (J)	11
Peak Power (kW)	227
Beam Sigma (cm)	0.25
Beam Spot (cm^2)	0.4
Beam Current (mA/cm^2)	159
Integrated Current ($\mu C/cm^2$)	8.0
Stopping Power (MeV/cm)	775
Energy Deposition (MW/cm^3)	123
Energy Deposition (kJ/cm^3)	6

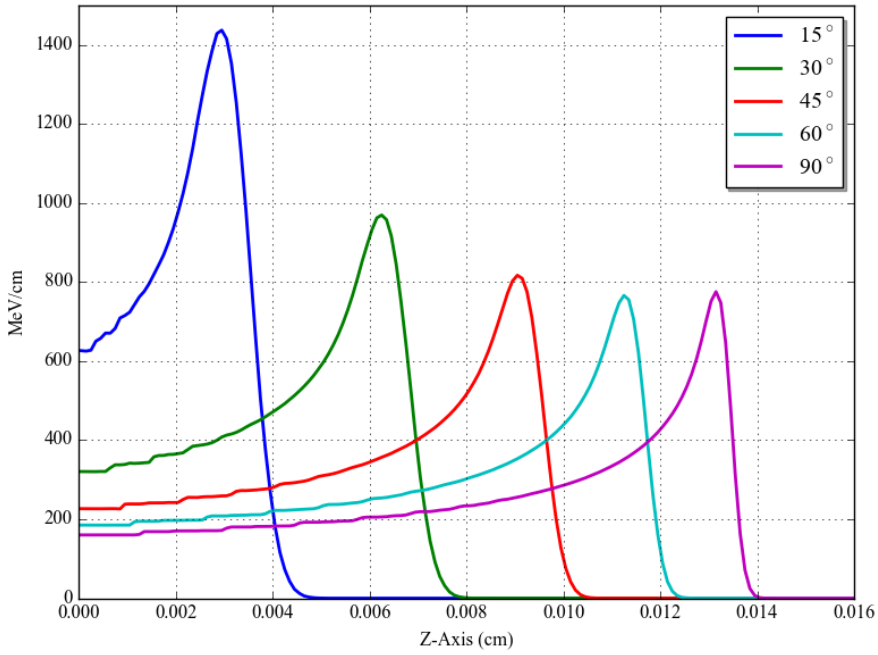

Figure 3: Stopping power for 3.63 MeV protons in Graphite as function of the incident angle.

3.2. **Thermo-Mechanical Results of Beam Irradiation**

In this section, we show the results for the beam conditions in the FC. For this purpose, we study the nominal conditions with a beam energy of 3.63 MeV, intensity of 62.5 mA, and pulse duration of 50 μs. For the FC we study a beam spot of σ_x=σ_y=2.5mm.

In Figure 4 we show the temperature stresses and deformations the FC, assuming perpendicular beam irradiation. The maximum temperature corresponds to the Bragg peak, at ~130 μm below the surface.

Regarding the stresses, compression (σ_3) appears at the irradiated zone. The maximum compression stresses appear in the Bragg peak. Below the irradiated zone (>150 μm), a tensile zone (σ_1) appears. The tensile zone is defined by boundary conditions and is up to 3 MPa in the FC. The stress intensity (σ_{Int}) both in the FC is dominated by compression stresses, which are much higher than tensile stresses.

Deformation in the FC, with symmetry conditions, will be less than 1 μm in the radial directions and ~1 μm in the axial direction.

In Figure 5 we show the evolution of temperature with time for a perpendicularly irradiated plate. The maximum temperature is attained at the end of the pulse (50 μs), then the graphite cools down. We observe that the temperature gets down almost completely in around 10 ms. The stresses, strains and deformations depend directly on the temperature and therefore follow a similar evolution.

In Table 3 we summarize the main thermo-mechanical conditions in the FC. For the FC, we show three cases: a perpendicular plate (FC:90º) and a plate with an incident angle of 45º (FC:45º) and 30º (FC:30º).

Regarding the stresses, we operate always below the design limit. In the case of a perpendicular FC, we operate 33% below the design limit. For a more conservative design, a 45º inclined plate would operate with 40% margin, and a 30º with a 46% margin.

Regarding the temperatures, the maximum temperature will be $T_{max.} = T_{steady} + \Delta T_{transient}$. In Section 4 we show that the steady state temperature keeps below 400 K. Therefore, the maximum temperature would be <1250 K for the faraday cup.

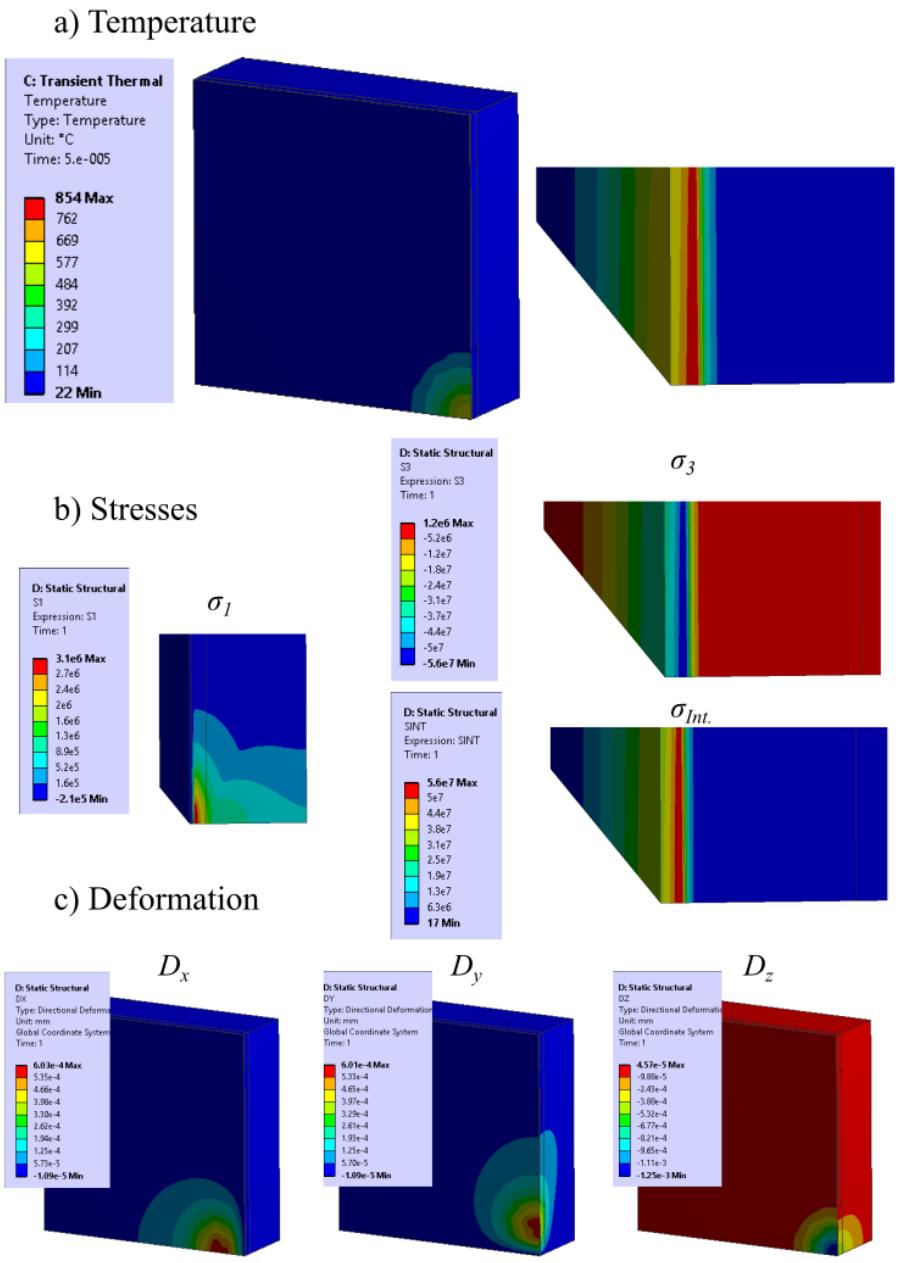

Figure 4: Temperature, stresses and deformations after beam irradiation (50 μs) in the FC assuming a perpendicular face of 90º.

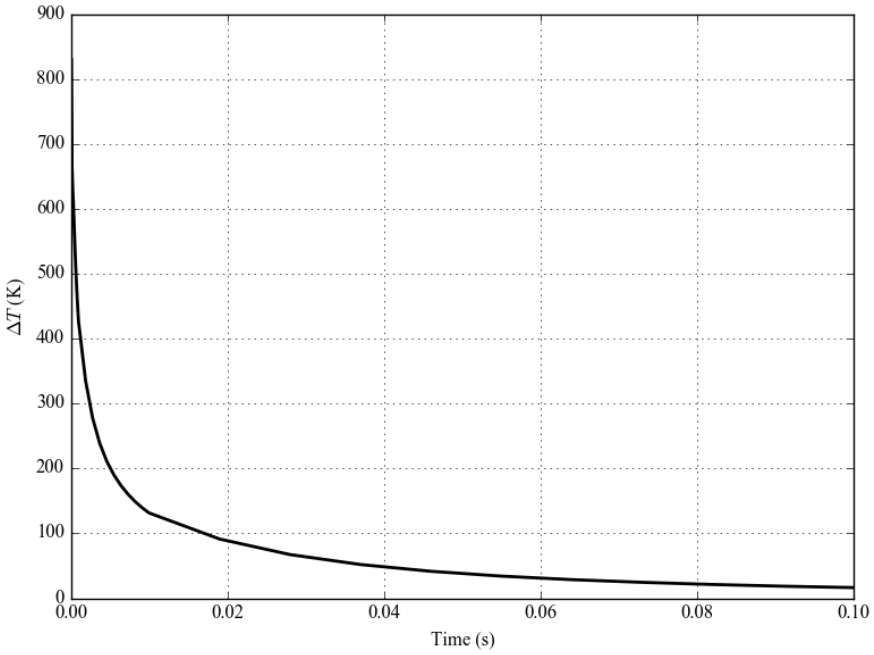

Figure 5: Maximum Temperature temporal evolution in the FC assuming a perpendicular face of 90º.

Table 3: Main thermo-mechanical conditions after beam irradiation (50 μm) in the FC.

Case	***I''* (μC/cm^2)**	**ΔT (K)**	**σ_1 (MPa)**	**σ_3 (MPa)**	**σ_{Int} (MPa)**	**$\sigma_{Int}/\sigma_{Lim.}$**	**Max. Def. (μm)**
FC: 90º	8.0	832	3.1	-56	56	67%	1.25
FC: 45º	5.6	731	2.3	-50	50	60%	0.88
FC: 30º	4.0	659	1.8	-44	45	54%	0.62

4. Steady State Analysis

4.1. Model Description

In this work, we have a Faraday Cup with a nominal diameter of 50 mm. In the FEM model we have simplified the CAD model in order to include only the graphite, insulator and substrate. Alumina (Al_2O_3) is chosen as the insulator material due to its excellent insulation capacities combined to acceptable thermal properties. In Figure 6 we show the geometry of the FEM model and in Table 4 the main dimensions are summarized.

For the refrigeration system, we used a channel of 4 mm internal diameter. Assuming cooling conditions with water at 300 K and flowing at ~1 m/s a film coefficient of h=5000 $Wm^{-2}K^{-1}$ is applied in the model [6], see also Cooling . For the thermal conditions, we have not included radiative effects.

For the support of the FC we apply null node displacement in the upper part of the model, corresponding to the joining with the actuators. We also apply symmetry conditions since only half of the Faraday Cup is simulated.

We apply a contact force in order to press the graphite against the substrate. A border contact between graphite, alumina and substrate is imposed in the external ring of the graphite surface with 2 mm width, see Figure 7. Structural simulations show that effective contact is only attained in the contact region, outside of the contact is minimum. We apply a contact model with a friction coefficient of 0.1[1]. This allows the different layers to slide over accommodate thermal expansions.

The thermal contact is defined by the model described in Appendix B: Thermal Contact Model. We have a thermal conductance of 0.0026 $WN^{-1}K^{-1}$ for the Gr-Al_2O_3-Cu contact and 0.0007 $WN^{-1}K^{-1}$ for Gr-Al_2O_3-Steel Contact.

The thermal load has been calculated introducing beam parameters (see Table 1) in a MCNPX model. The Bragg Peak for a 3.63 MeV proton beam in graphite is situated at ~130 μm and becomes null at ~140 μm. Since we are studying effects in the steady regime we homogenize the heat source in a mesh element of 140 μm. The beam size is defined by σ_x = 2.488 mm and σ_y=2.624 mm. In Figure 8 we show the heat load used in this work.

Table 4: FEM Model of the Faraday Cup: materials and main dimensions.

Parameter	Value	Parameter	Value
Coating Material	Graphite	FC Nominal Diameter	50 mm
Insulator Material	Alumina	Graphite Thickness	4 mm
Substrate Material	Steel/Copper	Alumina Thickness	1.5
		Substrate Thickness	17 mm
Water Channel Radius	2 mm	Contact Border	2 mm
Film Coefficient	5000 $Wm^{-2}K^{-1}$		
Water Temperature	300 K		

[1] http://www.engineeringtoolbox.com/friction-coefficients-d_778.html

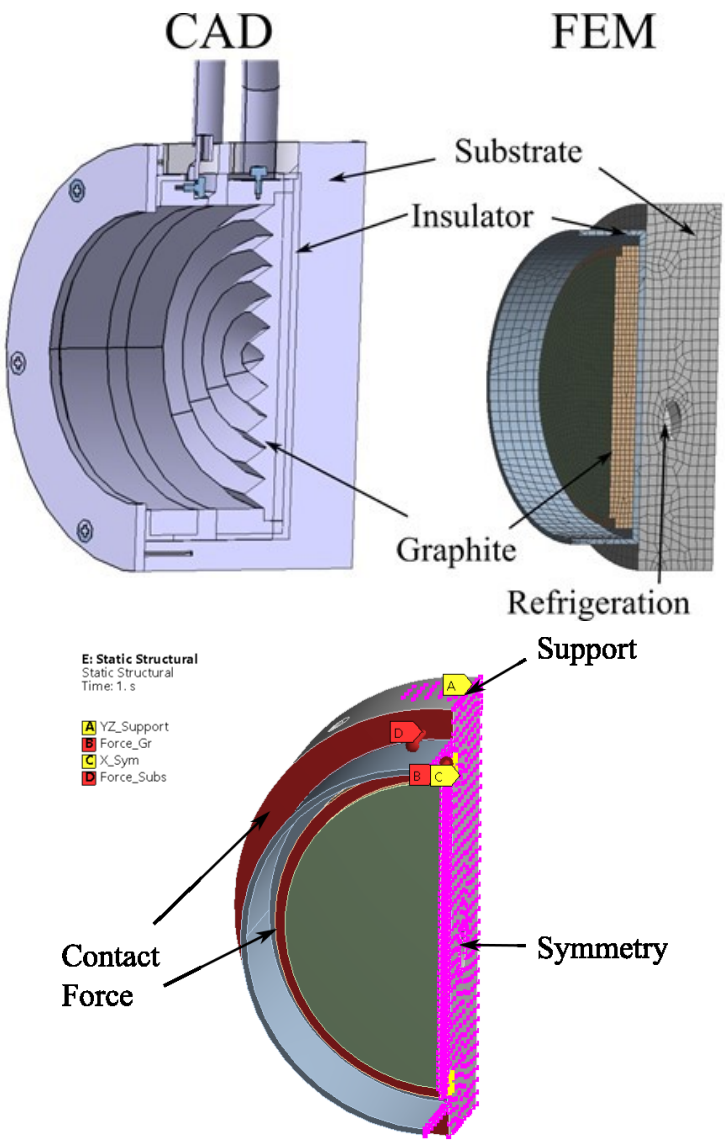

Figure 6: FEM model of the FC. Top) Geometry and mesh description. Bottom) Boundary conditions.

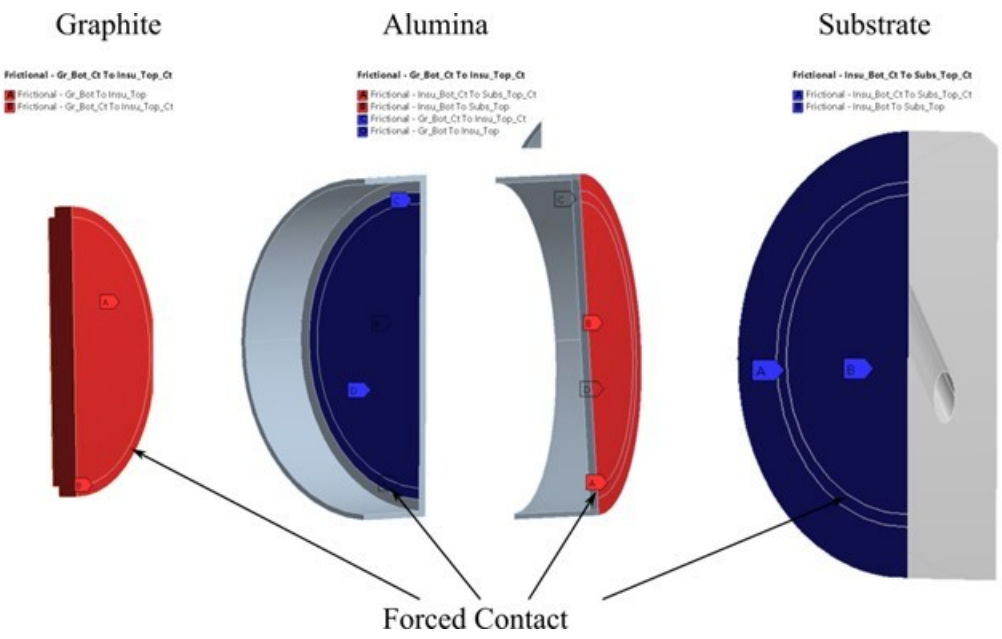

Figure 7: Contact Model of the FEM Model

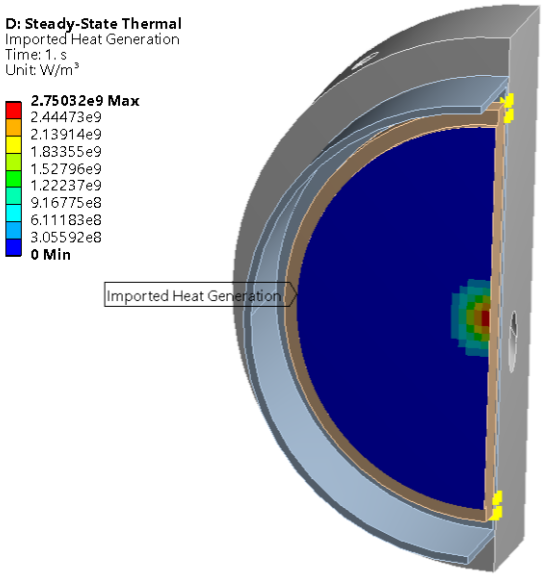

Figure 8: Thermal Load of the FEM Model as imported from the MCNPX simulations.

4.2. **Cooling System**

In this section, we describe the main parameters of the cooling system. We design the cooling system in order to have good heat transfer conditions with film coefficients of ~5000 W/m^{2}K in cooling channels of 4 mm of inner diameter.

In order to estimate the film coefficient we use Colburn equation [6]:

$$Nu = 0.023 \cdot Re_D^{4/5} \cdot \mathrm{Pr}^{1/3} \quad (4)$$

Where $Nu = h \cdot D/k$ is the Nusselt number, *Re* the Reynolds number and *Pr* the Prandtl number.

The pressure losses can be calculated as:

$$\Delta P = \frac{1}{2}\left(f\frac{L}{D} + K\right) \cdot \rho \cdot v^2 \quad (5)$$

Where *f* is the friction factor, *L* the equivalent pipe length, *D* the pipe diameter ρ the fluid density, *K* the singular losses and *v* the speed.

In order to have a quick estimation of the friction factor we can use explicit formulations such Haaland [7]:

$$\frac{1}{f^{1/2}} = -1.8 \cdot \log\left(\frac{6.9}{Re_D} + \left(\frac{\epsilon/D}{3.7}\right)^{1.11}\right) \quad (6)$$

Where *f* is the friction factor, *Re* the Reynolds number, ϵ is the pipe roughness and *D* the pipe diameter.

In order to have a preliminary estimation we can assume a roughness of ϵ=100 μm, tubing length of 2 m and singular losses K~20 [7].

In Table 5 we show the main heat transfer parameters. We observe that in order to obtain a film coefficient ~5000 W/m^{2}K in a channel of ϕ 4 mm we need water flowing at 1 m/s or ~0.75 l/min. For the pressure losses for this system, and we observe that they are in the range of 0.2 bars.

Table 5: Main parameters for the heat transfer and pressure losses of a water cooled channel.

Parameter	Value	Unit	Parameter	Value	Unit
ID	4	mm	*f*	0.06	
v	1	m/s	*L*	2	m
Q	1.75	l/min	$\Delta P_{friction}$	15230	Pa
			K	20	
Re	3988		$\Delta P_{singular}$	9899	Pa
Nu	33				
H	5008	W/m^2 K	ΔP	25219	Pa
				0.25	Bar

4.3. **Contact Force Parametric Analysis**

In the case of the Faraday Cup the temperature control is only important in order to guarantee good electrical insulation. Electric resistivity in alumina passes from $>10^{14}$ Ωm at 300 K to $\sim10^{12}$ at 500 K and $\sim10^{10}$ at 700 K [8]. Even if those values should also guarantee correct electrical insulation, is better to maximize insulation by controlling the system temperature. Therefore, we will aim for a design where the insulator is kept below ~400 K.

In Figure 9 we show the temperature variation as function of the contact force. In total, the temperature in the steady state is defined by the a) temperature gradient in the graphite, b) temperature gap in the contact region, c) temperature gradient in the substrate and d) temperature gap with the coolant (at 300K=. The temperature gradient in the graphite is ~20 K. The temperature gap in the graphite-insulator-substrate contact depends on the contact force and is represented by the dashes lines in Figure 9. We observe how for copper the contact temperature gap can be below 100 K for contact forces ~100K, while for Steel forces ~500 N should be applied. The temperature gradient in the substrate is ~20 K for SS and negligible (<1 K) in the case of copper. Finally, the temperature gap with the coolant is ~8 K.

In Figure 10 we show the deformations of the graphite as function of the contact force. Deformation tolerances are not critical in the FC, however we observe that they are small, below 30 μm in all cases for copper, and for forces >250 N in the case of a substrate steel.

In Figure 11 we show the maximum and minimum stresses in the graphite. For low contact forces (<100 N) the stresses are due to the thermal gradient and are small, <0.5 MPa. For higher contact forces, the stresses are due to the contact pressure, and can be -2 MPa for a contact force of 500 N.

From these results, in order to guarantee good thermal contact, contact forces ~100 N in case of a copper substrate and 500 N in the case of a steel substrate are recommended.

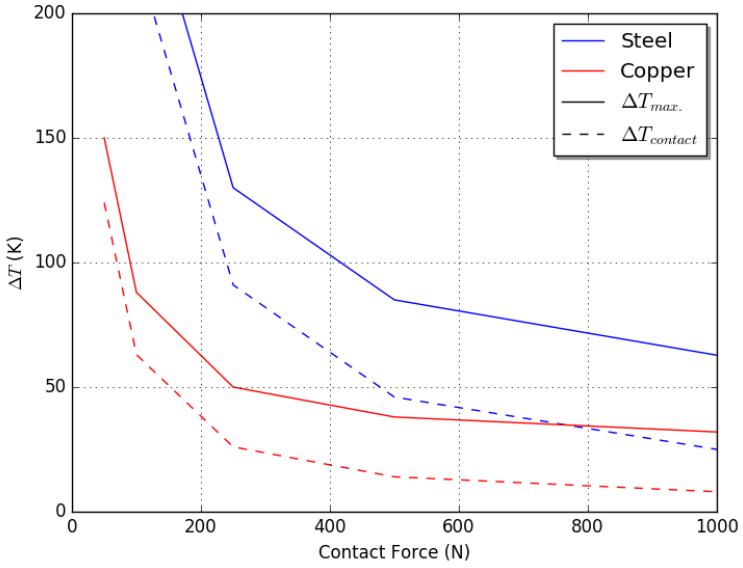

Figure 9: Temperature variation as function of the contact force.

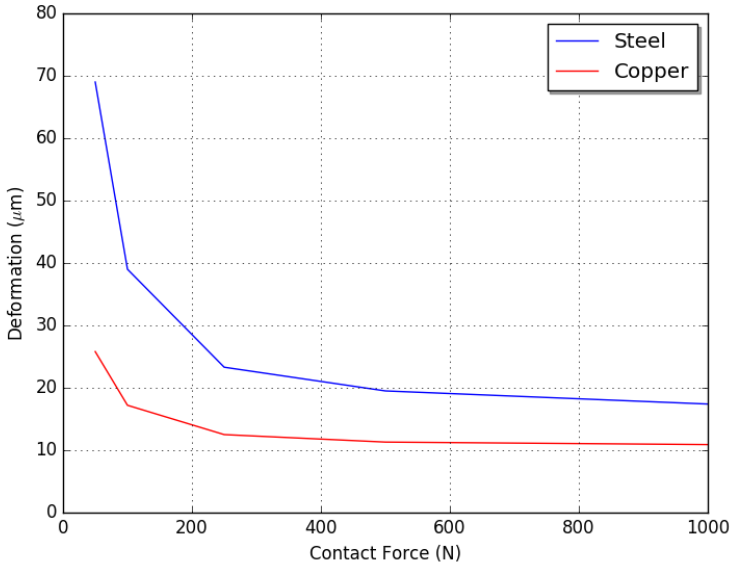

Figure 10: Graphite deformation as function of the contact force.

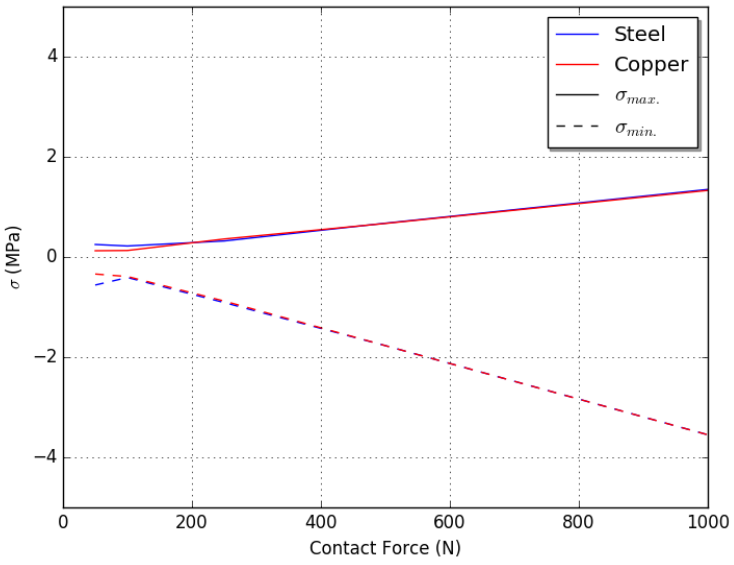

Figure 11: Graphite maximum and minimum stresses as function of the contact force.

4.4. **Thermo-Mechanical Results**

Next, we show the model results for *a)* copper substrate with a contact force of 100 N and *b)* steel substrate with a contact force of 500 N.

In Figure 12 the maximum temperature in the graphite after beginning of operation is shown. It is observed that the steady state is attained in 1000-2000 s.

In Figure 13, Figure 14 and Figure 15 the temperature, deformation and stresses and for cases with copper and steel substrate are shown. Figure 16 shows the contact pressure, it is observed that the contact is only effective in the contact areas. In the case of Copper-100N, since the force is lower, thermal effects play a role and the contact area is affected by the temperature distribution. This effect disappears and for higher forces where only the region where the force is applied is in contact.

After the analysis of the different contact conditions, a solution with a steel substrate and contact forces of 500 N has been chosen. For this chosen solution, in Figure 17 we show the stresses for the different components. For graphite and alumina, we show the stress intensity, and for steel the equivalent Von Mises Stress. In the cases of graphite collector, the stresses due to the steady state are <2 MPa, and for the insulator <70 MPa. In both cases the highest stresses take place in the contact region, and are much lower than the material strengths (~125 MPa for graphite and ~500 MPa for alumina, see Appendix A: Material Properties). For the steel substrate, the model shows that stresses up to ~70 MPa, may appear in the joining region, however these local stresses are due to the rigid boundary conditions of the model and will be different on the final joining design. In any case the stresses are also much lower than the yield strength of steel (~170 MPa). Therefore, we conclude that the different components will correctly operate in the steady state.

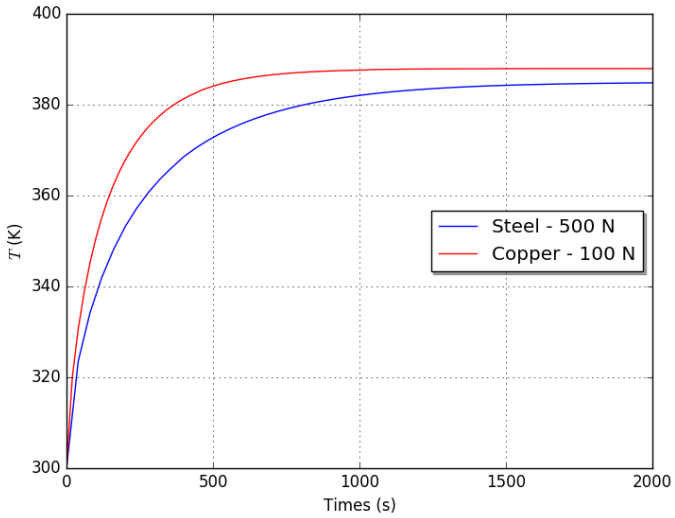

Figure 12: Temperature transient after the start-up.

Cu - 100 N Steel - 500 N

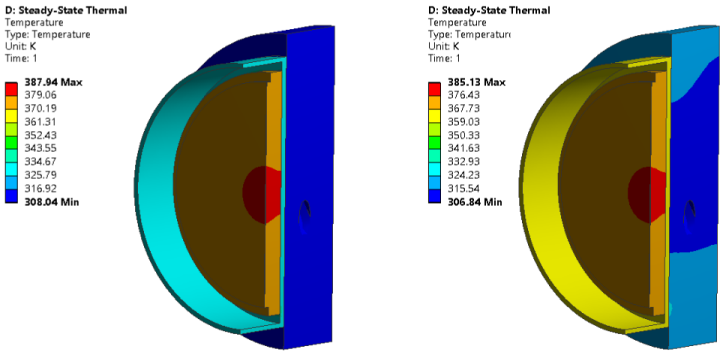

Figure 13: Temperature contours for left) Cu substrate with a contact force of 100 N and right) Steel substrate with a contact force of 500 N.

Cu - 100 N Steel - 500 N

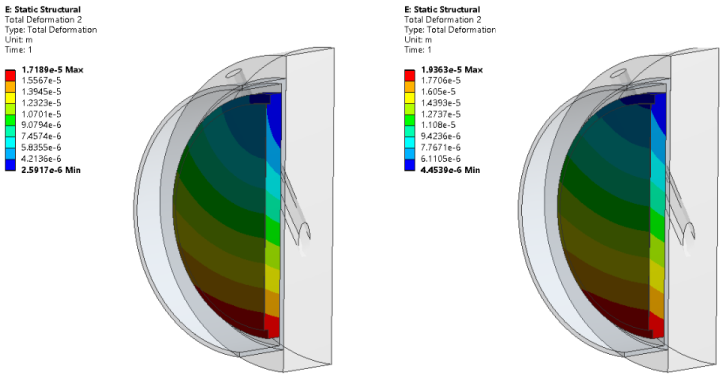

Figure 14: Total Deformation contours for left) Cu substrate with a contact force of 100 N and right) Steel substrate with a contact force of 500 N.

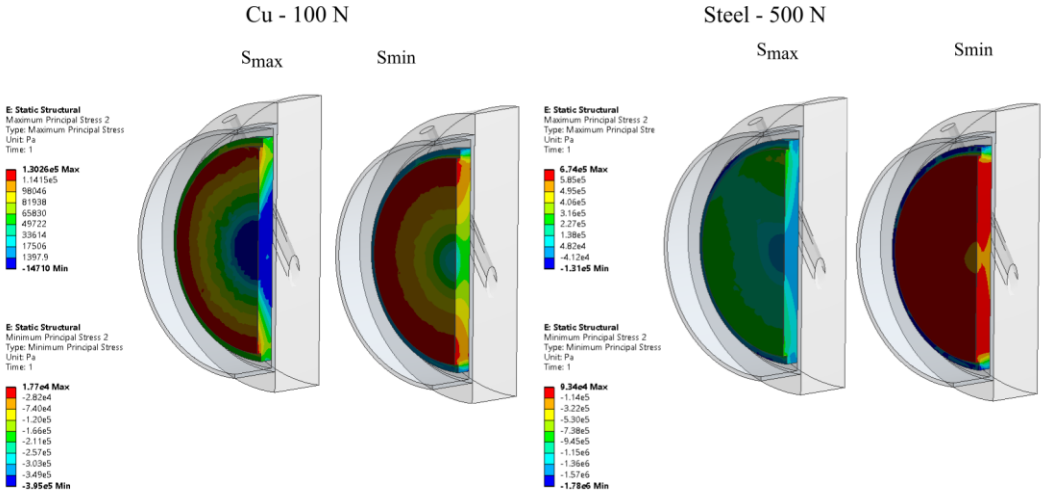

Figure 15: Principal stresses contours for left) Cu substrate with a contact force of 100 N and right) Steel substrate with a contact force of 500 N.

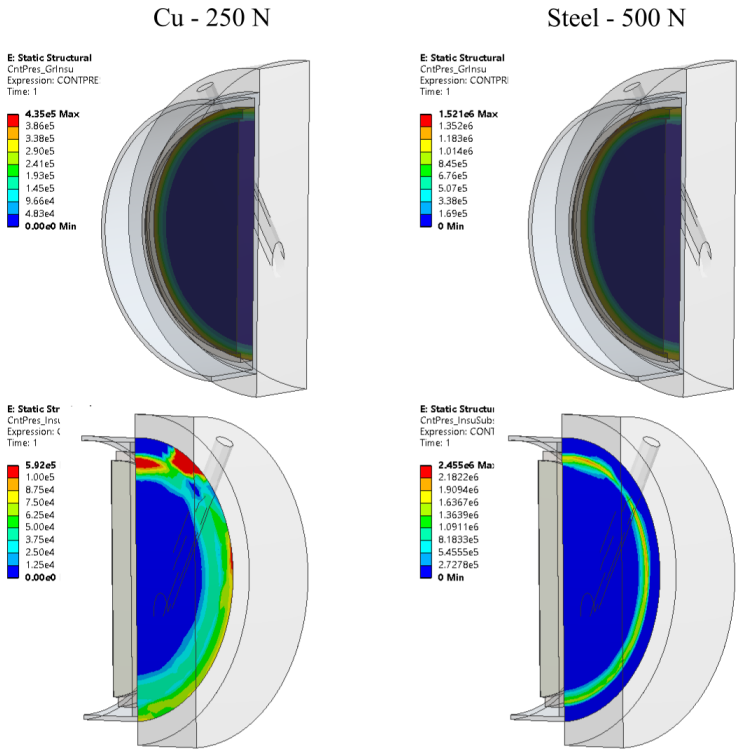

Figure 16: Contact pressure contours for left) Cu substrate with a contact force of 100 N and right) Steel substrate with a contact force of 500 N. The top figures represent Gr-Alumina contact and the lower Alumina-Substrate contact.

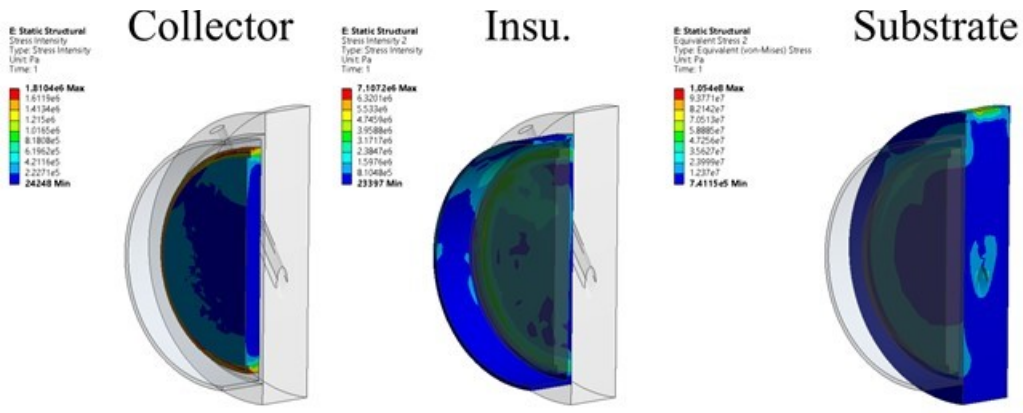

Figure 17: Intensity (Collector and Insulator) and Von Mises (Substrate) stresses for the different components of the Faraday Cup.

5. **Transient + Steady State Analysis**

In this simulation, we show results of graphite irradiation at the temperature attained during the steady state operation. For this purpose, we study irradiation with use the model described in Section 3 at the steady state temperature described in Section 4

In Figure 18 we show the temperature profile for a graphite plate with irradiation at 30º. In Table 3 we show the results and compared it with irradiation at room temperature of Section 3. As expected the results are similar, the small temperature in the temperature variation is due to the increase of the specific heat from room temperature (300 K) to the steady state temperature (~400 K) for a case with a steel substrate and contact forces of 500 N.

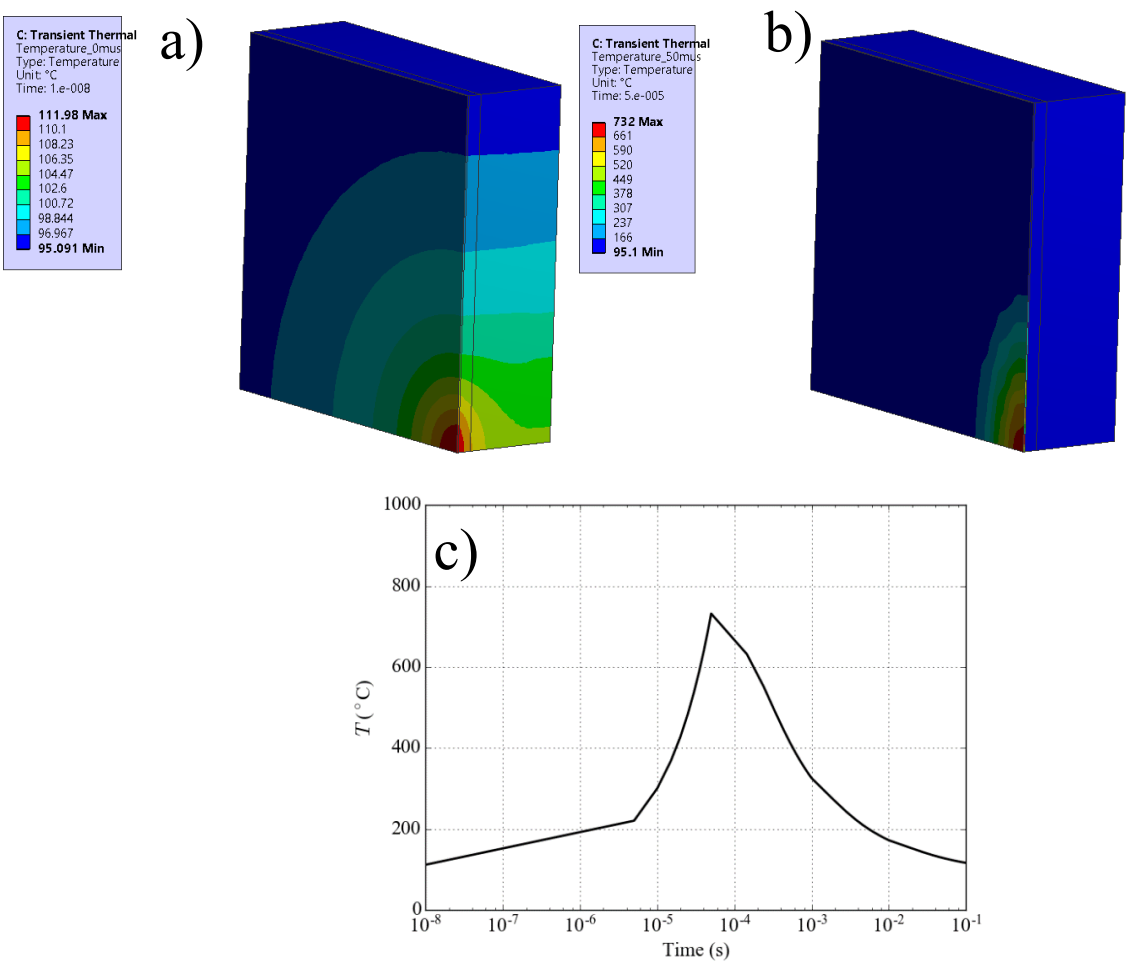

Figure 18: Temperature contour for the Steady + Transient model. a) The temperature profile in the steady state, b) temperature profile after the pulse irradiation (50 μs), c) temperature evolution of the irradiated surface during and after beam irradiation.

Table 6: Main thermo-mechanical conditions after beam irradiation (50 μm) in the FC. Case for graphite inclination at 30º.

Case	I'' (μC/cm^2)	ΔT (K)	σ_1 (MPa)	σ_3 (MPa)	σ_{Int} (MPa)	$\sigma_{Int}/\sigma_{Lim.}$
Transient at Initial (300 K)	4.0	659	1.8	-44	45	54%
Transient at Steady (385 K)	4.0	620	1.6	-44	44	53%

6. **Conclusions**

In this work, we study thermo-mechanical effects for operation in the FC of the MEBT line. We study its behaviour for the operational conditions expected during MEBT commissioning phase. First, we study beam irradiation of the graphite (Section 3) collector and then the steady state operation (Section 4).

The beam irradiation transient is characterized by material heating and expansion which leads to compressive stresses during pulse irradiation. The maximum temperature and stresses take place in the Bragg Peak, and depend on the energy deposition and heat diffusion.

We study the behaviour during the irradiation pulse, studying how the maximum temperatures and stresses in the irradiated graphite are lower than the design limits. In Table 7 we summarize the main results of the work. We observe how for the FC with inclined faces of 30º we operate at ~50 % of the design limit.

For the steady state we specifically address the use of copper or steel as the substrate material. We show that, depending on the contact force, they can have give similar performances. The main difference is observed in the thermal contact, requiring higher contact forces for steel, which we specify to be at least 500 N. With this contact specification, we guarantee that the maximum temperature is below 400 K and the insulation properties are not largely affected.

In Table 7 we summarize the conditions of operation for the proposed solutions for FC.

Table 7: Main thermo-mechanical conditions in the graphite collector for indentation at 30º, steel substrate and contact forces of 500 N.

Case	ΔT **(K)**	σ_1 **(MPa)**	σ_3 **(MPa)**	σ_{Int} **(MPa)**	$\sigma_{Int}/\sigma_{Lim.}$	**Max. Def. (µm)**
Initial	300	0	0	0	0	0
Transient at Initial (300 K)	659	1.8	-44	45	54%	0.6
Transient at Steady (385 K)	620	1.6	-44	44	53 %	0.6
Steady	85	0.7	-1.8	1.8	2 %	20
Total (Init. + Steady + Transient)	1005	1.6	-44	44	53%	20

Appendix A: Material Properties

In this model we use Graphite R4550 with material properties obtained from Linac 4 Cern Group, and reported in Refs. [2, 4], we obtain its hardness from Ref. [5]. For Steel we use SS316L properties reported in Ref. [9] with strength limits from Ref. [10] and microhardness from Ref. [11]. For copper we use pure copper properties reported in Ref. [9] with strength limits from Ref. [12]. For alumina we use the properties reported in Refs. [12, 13] for Alumina of 99.9% purity.

The material properties of the materials used in the work are summarized in Table 8.

Table 8: Material properties for Graphite R4550 [2, 4, 5] , SS316 [9–11], pure copper [9, 12] and alumina 99.9% [12, 13].

Mat. Limit	**Graphite**	**Steel**	**Copper**	**Alumina**
Max. Temp. (K)	3773	1700	1357	2000
Ult. Tensile Strength (MPa)	40	450	209	552
Ult. Comp. Strength (MPa)	125			
Yield Strength (MPa)	-	170	33	
Young Modulus (GPa)	11.7	200	125	386
Poisson Coefficient	0.15	0.3	0.343	0.22
Thermal Conductivity, at 300 K (W $m^{-1}K^{-1}$)	103	14	398	39
Density, at 300 K (kg m^{-3})	1800	7930	8930	3960
Specific Heat, at 300 K (J kg^{-1} K^{-1})	824	472	385	880
Coefficient of thermal expansion, at 300 K (μm m^{-1} K^{-1})	4	15	16	8

Appendix B: Thermal Contact Model

In this section, we describe the thermal contact model used in this work.

We apply the model to the contact regions. In the regions where not mechanical contact is expected we assume adiabatic conditions.

In our case we model conforming rough contacts, where the contact thermal conductance (h_c) is dependent conductivity (k), roughness (σ/m) and micro-hardness (H_c) of contact materials. For the analysis we use Yovanovich's model [11, 14–17]:

$$h_c \cdot \frac{\sigma_c/m_c}{k_c} = 1.25 \cdot \left(\frac{P}{H_c}\right)^{0.95} \quad (7)$$

Since we want to study the thermal contact as function of the contact force we have linearized the previous equation. This results in a conservative estimation of the contact conductance as function of the force, obtaining h_c/P in $WN^{-1}K^{-1}$.

$$h_c \cdot \frac{\sigma_c/m_c}{k_c} \lesssim 1.25 \cdot \left(\frac{P}{H_c}\right) \quad (8)$$

$$\frac{h_c}{P} \lesssim 1.25 \cdot \frac{k_c}{\sigma_c/m_c} \cdot \frac{1}{H_c}$$

Where k_c is the contact conductivity that can be estimated as the harmonic mean of both materials [14, 15]:

$$k_c = \frac{k_1 \cdot k_2}{(k_1 + k_2)/2} \quad (9)$$

The surface roughness, σ, and the asperity slope, m, can be related as [15]:

$$m = 1.52 \cdot \left(\frac{\sigma}{1\mu m}\right)^{0.4} \quad (10)$$

In order to calculate the contact roughness $\sigma_c^2 = \sigma_1^2 + \sigma_2^2$ and $m_c^2 = m_1^2 + m_2^2$ [14, 15].

For the microhardness H_c the softer of the two materials is taken [11, 14].

In the case of metals, the microhardness H_c can be can be calculated as [11, 16].

$$H_c = C_1 \cdot \left(1.62 \cdot 10^6 \cdot \frac{\sigma}{m}\right)^{C_2} \quad (11)$$

Where C_1 and C_2 are the Microhardness Vickers coefficients. C_2 ~ -0.26 for most materials [11]. C_1=6906 MPa for steel [11]. Since for metals hardness is proportional to the tensile strength, $H \sim 3\sigma_u$ [15, 18, 19], we estimate C_1 for copper as 3207 MPa.

In the case of non-metals (alumina, graphite), hardness is larger than the tensile stress ($H \gg 3\sigma_u$). Therefore, in order to calculate C_1 we will extrapolate from macro-hardness using Eq. (11), and assuming the curve intersects with macrohardness at σ =700 μm [2]. Using this method we have a macrohardness for Al_2O_3 of 15 GPa [12] and C_1=77 GPa. For graphite we have a macrohardness of $90HR_{5/100}$ [5], which can be approximated to ~737 MPa [20] and from which we obtain C_1=3700 MPa. In Table 9 we summarize the macro and micro-hardness parameters used in this model.

In Ref. [4] a contact conductance for Gr-Cu of $\boldsymbol{h_c/P}$**~0.0145 WN^{-1}K^{-1}** , which is in agreement with our model if we assume a roughness σ = 1.6 μm.

Under the conditions assumed in our model, for Gr-Steel we estimate a contact conductance h_c/P~0.002 WN^{-1}K^{-1}. This is 7 times lower than for Gr-Cu and therefore Gr-Steel will need of contact forces 7 times higher than Gr-Cu in order to have a similar thermal behaviour.

In the case of contacts with alumina, we estimate conductances of 0.0044 WN^{-1}K^{-1} for Gr-Al_2O_3, 0.0009 WN^{-1}K^{-1} for Al_2O_3-SS and 0063 WN^{-1}K^{-1} for Al_2O_3-Cu. Which means that the most restrictive contact would be SS-Al_2O_3 with conductance around 7 times worse than Cu-Al_2O_3.

In the case of several contact pairs the total conductance is calculated as $\frac{1}{h} = \frac{1}{h_1} + \frac{1}{h_2}$. Therefore Gr-$Al_2O_3$-SS results in a conductance of 0.0007 WN^{-1}K^{-1} and Gr-Al_2O_3-Cu in 0.0026 WN^{-1}K^{-1}

In Table 10 we show the thermal conductance and resistance for different contact pairs in our model. It is important to point out that these values correspond to the model described in this section, which depends on many parameters (material hardness, roughness, conductivity, plastic contact behaviour, etc). We have compared our model to the Gr-Cu contact given in Ref. [4], for the rest of contact pairs the results should give qualitative trends of the contact behaviour as function of the materials.

Table 9: Hardness parameters of the model.

	Graphite	**Steel**	**Copper**	**Alumina**
Macrohardness (MPa)	713	1350	627	15000
Microhardness, C_1 (MPa)	3700	6906	3207	77000

Table 10: Thermal Contact Conductance and Resistance of the model.

	Conductance (WN^{-1}K^{-1})	**Resistance (KNW^{-1})**
Gr-Cu	0.0146	69
Gr-SS	0.0019	517
Gr-Al_2O_3	0.0044	230
Al_2O_3-Cu	0.0063	159
Al_2O_3-SS	0.0009	1159
Gr- Al_2O_3-Cu	0.0026	388
Gr- Al_2O_3-SS	0.0007	1388

[2] This is the roughness for microhardness intersection with macrohardness that appears for our model in the case of metals.

Appendix C: Screw Tightening

In this work, we conclude that contact forces of ~500 N are required for the FC. In the FC, the design includes 6 screws, therefore each screw requires 85 N.

As a general approximation, the tightening torque depends on the pitch of the screw and on the friction in the thread and the screw head. As a general approximation, the torque can be calculated as [15]:

$$T = \left(\frac{p \cdot F}{2\pi} + 0.58 \cdot \mu \cdot d_2 + \mu_b \cdot r_m\right) \quad (12)$$

Where F is the contact force, p is the screw pitch, d_2 is the screw mean diameter, r_m is the mean radius in the screw head, μ is the friction factor in the thread and μ_b the friction factor in the head.

Therefore, the required torque depends a lot on the screws chosen for the design. The proposed design for the FC uses ISO 4762 M2 screws [3]. For these screws p=0.4 mm, d=2 mm, r_m =1.45 mm. Standard friction coefficients for steel-steel contacts[4] are slightly below 1, so we can assume μ=μ_b=1. With the previous assumptions a tightening torque of 0.22 Nm would be necessary for the FC.

The recommended seating torque for ISO 4762 screws is ~0.5 Nm for M2 [5]. Tightening with this torque would result in contact pressures ~4 MPa, which is lower than the strength of graphite. Therefore, fastening the screws with the recommended torque will result in adequate contact conditions.

Since the correspondence of screw torque and force depends greatly on geometry and friction, a calibration of the torque-force relation can be done using disc spring. For example, disc springs DIN 2093[6] offer contact forces of 50-100 N.

[3] http://www.fasteners.eu/standards/ISO/4762/

[4] http://www.engineeringtoolbox.com/friction-coefficients-d_778.html

[5] http://fullerfasteners.com/tech/torque-information/

[6] http://schnorr.com/download/schnorr-product-range/?wpdmdl=94

References

[1] D. de Cos et al., “Preliminary design of the ESS MEBT Faraday Cup,” Jul-2016.

[2] T. Mora, I. Bustinduy, and F. Sordo, “ESS-Bilbao Beam Stoppers criteria (MEBT-BI-FC04-02),” 16-May-2016.

[3] M. Munoz, M. Eshraqi, A. Jansson, S. Molloy, and M. Lindroos, “Description of Modes for ESS Accelerator Operation,” Internal ESS ESS-0038258 Rev. 3 Prelminary State, Nov. 2015.

[4] F. Carra and A. Dallochio, “LINAC4 3MeV test stand: Thermo-mechanical analysis of the Slit,” CERN, CERN CH1211 Geneva 23 Switzerland, CERN Internal Report 1102149 0.1, Nov. 2010.

[5] SGL Group: The Carbon Company, “Specialty Graphites for the Metal Industry,” SGL Group, Commercial Brochure.

[6] F. P. Incropera, D. P. DeWitt, T. L. Bergman, and A. S. Lavine, *Fundamentals of Heat and Mass Transfer*, Edición: 6th ed. Hoboken, NJ: Wiley John + Sons, 2006.

[7] F. White, *Fluid Mechanics*, 7 edition. New York, N.Y.: McGraw-Hill Education, 2010.

[8] P. Auerkari, “Mechanical and physical properties of engineering alumina ceramics.,” VTT Manufactoring Technology, Technical Research Center of Finland, Research Notes 1792, 196AD.

[9] Y. Lee and M. Hartl, “ESS Target Materials Handbook,” Internal ESS ESS-0028465, Feb. 2016.

[10] ASM, Ed., *ASM andbook Volume 1: Properties and Selection: Irons, Steels, and High-Performance Alloys*, 10 edition. Materials Park: ASM International, 1990.

[11] S. Song and M. Yovanovich, “Explicit relative contact pressure expression - Dependence upon surface roughness parameters and Vickers microhardness coefficients,” 1987.

[12] ASM, *ASM Handbook Volume 2: Properties and Selection : Nonferrous Alloys and Special-Purpose Materials*, 10th edition. Place of publication not identified: ASM International, 1990.

[13] “Aluminum Oxide | Al2O3 Material Properties.” http://accuratus.com/alumox.html.

[14] M. M. Yovanovich, J. R. Culham, and P. Teertstra, “Calculating interface resistance,” *Electron. Cool.*, vol. 3, no. 2, pp. 24–29, 1997.

[15] A. K. Hasselström and U. E. Nilsson, “Thermal contact conductance in bolted joints,” 2012.

[16] M. M. Yovanovich, “Micro and Macro Hardness Measurements, Correlations, and Contact Models,” presented at the 44th AIAA Aerospace Sciences Meeting and Exhibit, Reno, Nevada, 2006, vol. AIAA 2006-979.

[17] M. Bahrami, J. R. Culham, and M. M. Yovanovich, “Modeling Thermal Contact Resistance: A Scale Analysis Approach,” *J. Heat Transf.*, vol. 126, no. 6, pp. 896–905, Jan. 2005.

[18] P. Zhang, S. X. Li, and Z. F. Zhang, “General relationship between strength and hardness,” *Mater. Sci. Eng. A*, vol. 529, pp. 62–73, Nov. 2011.

[19] E. J. Pavlina and C. J. V. Tyne, “Correlation of Yield Strength and Tensile Strength with Hardness for Steels,” *J. Mater. Eng. Perform.*, vol. 17, no. 6, pp. 888–893, Apr. 2008.

[20] DIN51917, “Rockwell hardness of carbonaceous materials by the steel ball indentation method.” DIN, 1997.